OPEN

Citation: Cell Death and Disease (2014) 5, e1362; doi:10.1038/cddis.2014.331

www.nature.com/cddis

PARP1 activation/expression modulates regional-specific neuronal and glial responses to seizure in a hemodynamic-independent manner

J-E Kim[1], Y-J Kim[1], JY Kim[1] and T-C Kang*[,1]

Poly(ADP-ribose) polymerase-1 (PARP1) plays a regulatory role in apoptosis, necrosis and other cellular processes after injury. Status epilepticus (SE) induces neuronal and astroglial death that show regional-specific patterns in the rat hippocampus and piriform cortex (PC). Thus, we investigated whether PARP1 regulates the differential neuronal/glial responses to pilocarpine (PILO)-induced SE in the distinct brain regions. In the present study, both CA1 and CA3 neurons showed PARP1 hyperactivation-dependent neuronal death pathway, whereas PC neurons exhibited PARP1 degradation-mediated neurodegeneration following SE. PARP1 degradation was also observed in astrocytes within the molecular layer of the dentate gyrus. PARP1 induction was detected in CA1–3-reactive astrocytes, as well as in reactive microglia within the PC. Although PARP1 inhibitors attenuated CA1–3 neuronal death and reactive gliosis in the CA1 region, they deteriorated the astroglial death in the molecular layer of the dentate gyrus and in the stratum lucidum of the CA3 region. *Ex vivo* study showed the similar regional and cellular patterns of PARP1 activation/degradation. Taken together, our findings suggest that the cellular-specific PARP1 activation/degradation may distinctly involve regional-specific neuronal damage, astroglial death and reactive gliosis in response to SE independently of hemodynamics.
Cell Death and Disease (2014) **5,** e1362; doi:10.1038/cddis.2014.331; published online 7 August 2014

Poly(ADP-ribose) polymerase-1 (PARP1) repairs single-stranded DNA (ssDNA) breaks following various injuries. As PARP1 utilizes NAD^+ to form poly(ADP-ribose) polymers (PAR) during this process, extensive PARP1 activation results in energy failure, promoting necrotic cell death because of NAD^+ depletion.[1–6] Furthermore, PARP1 is a useful hallmark of apoptosis because full-length PARP1 is cleaved by the apoptotic proteases, caspase-3 and -7, into p85 and p25 fragments during apoptosis.[7,8] In contrast, the degradation of full-length PARP1 protein without cleavage into apoptotic fragments is mediated by caspase-independent ubiquitylation that plays a regulatory role in apoptosis, necrosis and other PARP1-regulated cellular processes.[9–12] Therefore, it is likely that the distinct profiles of PARP1 (activation, cleavage or degradation) may involve the differential cellular responses following harmful stimuli.

Status epilepticus (SE) is a medical emergency with significant mortality.[13] SE is a continuous seizure activity involving severe and prolonged hypoxia that induces sustained neuronal damage, astroglial death and reactive astrogliosis.[14–23] In particular, astroglial responses show regional-specific patterns following SE. Briefly, astroglial death was observed in the molecular layer of the dentate gyrus and the piriform cortex (PC) before or after neuronal death. In contrast, reactive astrogliosis was detected in other regions of the hippocampus and cortex.[19–25] Based on the properties of PARP1 responses to stimuli, it is likely that PARP1 may be one of the potential molecules to involve neuronal damage and regional-specific astroglial responses to SE. In order to address this hypothesis, we first investigated the characteristics of PARP1 responses to SE in the rat hippocampus and PC. We then examined whether PARP1 regulates the neuronal/glial responses to SE, and finally whether hemodynamics involves PARP1 responses to SE using *ex vivo* model.

Results

PARP1 differently involved neuronal and astroglial responses to SE in the hippocampus. Western blot data revealed that SE reduced the level of full length of PARP1 protein without cleavage into apoptotic fragments in the hippocampus 2–3 days after SE (Figures 1a and b, $P<0.05$ *versus* non-SE animals). At 1 to 4 weeks after SE, the level of full length of PARP1 protein in the hippocampus was increased as compared with that observed at 3 days after SE, whereas it was still lower than that observed in non-SE animals (Figures 1a and b, $P<0.05$ *versus* 3 days after SE). As compared with non-SE animals, the number of PARP1-positive CA1 and CA3 neurons (not dentate granule cells) was reduced 3 days after SE (Figures 1c and d, $P<0.05$ *versus* non-SE animals). At 1 week after SE, the number of PARP1-positive CA1 and CA3 neurons was similar to that observed 3 days after SE. In contrast to neurons, SE induced

[1]Department of Anatomy and Neurobiology, Institute of Epilepsy Research, College of Medicine, Hallym University, Chunchon, South Korea
*Corresponding author: T-C Kang, Department of Anatomy and Neurobiology, College of Medicine, Hallym University, Chunchon 200-702, Kangwon-Do, South Korea. Tel: +82 33 248 2524; Fax: +82 33 248 2525; E-mail: tckang@hallym.ac.kr
Abbreviations: PARP1, poly(ADP-ribose) polymerase-1; PAR, poly(ADP-ribose) polymers; SE, status epilepticus; PC, piriform cortex; FJB, Fluoro-Jade B; ACSF, artificial cerebrospinal fluid; PILO, pilocarpine; SD, Sprague-Dawley; PB, phosphate buffer; PBS, phosphate-buffered saline; SDS, sodium dodecyl sulfate
Received 10.3.14; revised 10.6.14; accepted 03.7.14; Edited by A Verkhratsky

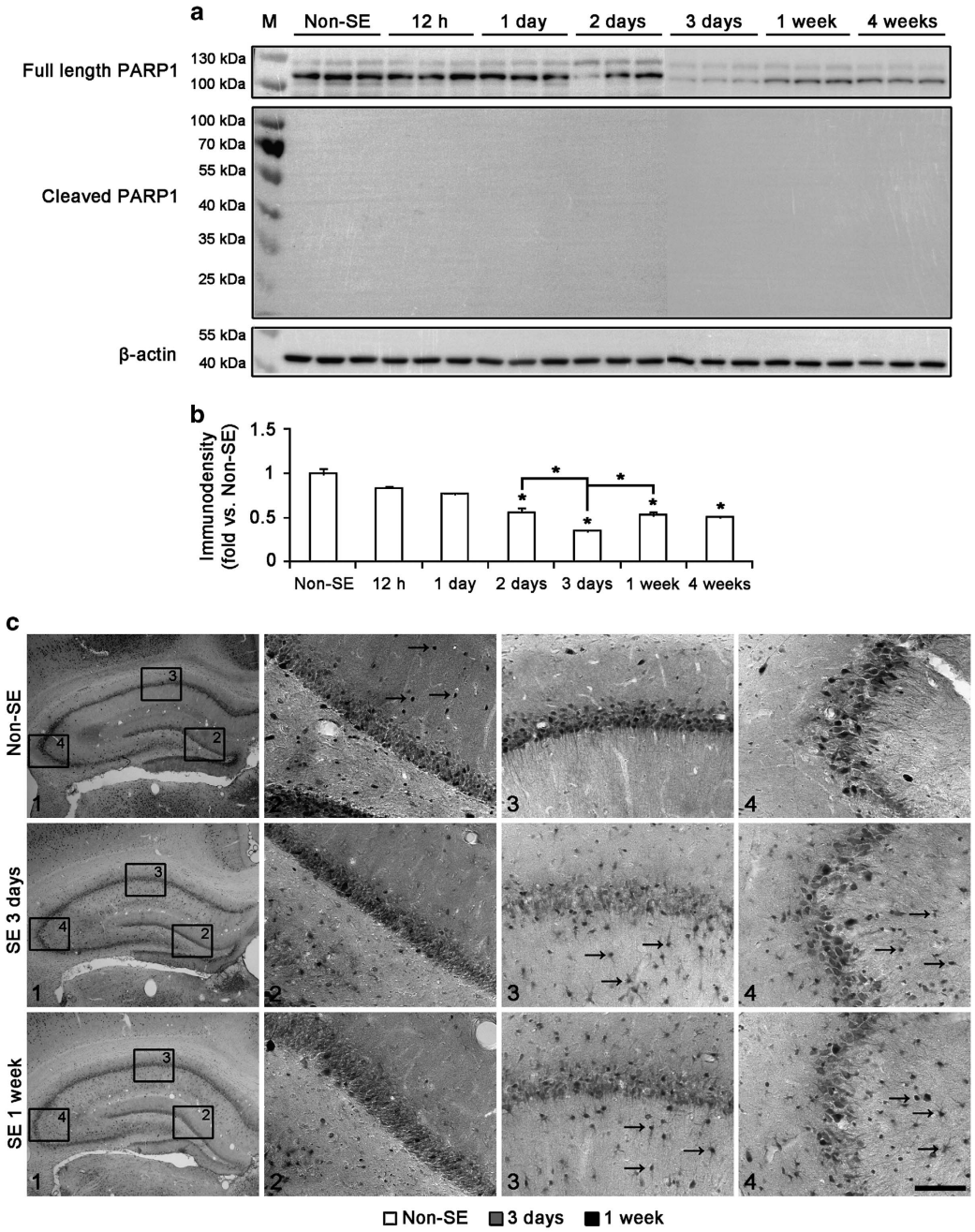
a
M
Non-SE
12 h
1 day
2 days
3 days
1 week
4 weeks
Full length PARP1
130 kDa
100 kDa
Cleaved PARP1
100 kDa
70 kDa
55 kDa
40 kDa
35 kDa
25 kDa
β-actin
55 kDa
40 kDa
b
Immunodensity (fold vs. Non-SE)
1.5
1
0.5
0
Non-SE
12 h
1 day
2 days
3 days
1 week
4 weeks
c
Non-SE
SE 3 days
SE 1 week
1
2
3
4
Non-SE
3 days
1 week
d
Number of PARP1 neurons/10⁵ μm²
4000
3000
2000
1000
0
DG
CA1
CA3

PARP1 expression in non-neuronal cells within the stratum radiatum of CA1 and the stratum lucidum of CA3 region at 3 days to 4 weeks after SE. However, SE diminished PARP1 expression in non-neuronal cells within the molecular layer of the dentate gyrus (Figure 1c). Double immunofluorescent study revealed that non-neuronal cells showing PARP1 expression in the molecular layer of the dentate gyrus were astrocytes (Figure 2a). Consistent with previous studies,[19,24] SE resulted in apoptotic astroglial death accompanied by disappearance of PARP1, GFAP and glutamine synthase (GS) expression in the molecular layer of the dentate gyrus (Figures 2a, b and d, $P<0.05$ *versus* non-SE). In contrast to the dentate gyrus, reactive astrocytes showed PARP1 induction in the CA1–3 regions following SE (Figures 2c and d, $P<0.05$ *versus* non-SE).

SE degraded PARP1 in PC neurons, but induced it in microglia in the PC. Similar to the hippocampus, the level of full length of PARP1 protein was gradually reduced in the PC without cleaved PARP1 fragments until 3 days after SE (Figures 3a and b, $P<0.05$ *versus* non-SE animals). At 1 to 4 weeks after SE, the level of full length of PARP1 protein in the PC was increased as compared with that observed at 3 days after SE, whereas it was still lower than that observed in non-SE animals (Figures 3a and b, $P<0.05$ *versus* 3 days after SE). In non-SE animals, PARP1 expression was obviously detected in neurons, but not in non-neuronal cells (Figures 3c and d). Following SE, the number of PARP1-positive neurons was reduced in the PC as compared with non-SE animals, although PARP1 induction was detected in non-neuronal cells (Figure 3c). SE resulted in massive astroglial death in the PC and PARP1 degradation in PC neurons (Figures 4a–c). Reactive astrocytes in the PC showed no PARP1 induction (data not shown). In contrast, IB4-positive microglia exhibited strong PARP1 expression following SE (Figure 4b). Together with changed PARP1 expression in the hippocampus, our findings indicate that PARP1 degradation/induction may show the regional and cellular-specific patterns in the rat hippocampus and the PC following SE.

PARP1 activity was observed in hippocampal neurons and CA1-reactive astrocytes following SE. To elucidate the correlation between PARP1 activity and cellular responses to SE, we examined PARP1 activity by immunohistochemistry for PAR. In non-SE animals, PAR immunoreactivity was rarely observed in the hippocampus or the PC. At 12 h after SE, PAR immunoreactivity was detected in CA1–3 neurons and dentate granule cells. In contrast, few PC neurons showed PAR induction (Figure 5). At 1 day to 4 weeks after SE, PAR immunoreactivity was gradually reduced in CA1–CA3 neurons, dentate granule cells and PC neurons (data not shown). PAR induction was detected in some astrocytes within the stratum radiatum of CA1 region (Figure 5). These findings indicate that PARP1 activity may involve hippocampal neuronal death and CA1-reactive astrocytes following SE.

PARP1 inhibitor attenuated neuronal damage and reactive astrogliosis, but aggravated astroglial death following SE. To confirm the role of PARP1 activity in SE-induced neuron–astroglial damage, we applied PJ-34 and DPQ (PARP1 inhibitors) before SE induction. In the vehicle-treated group, the numbers of Fluoro-Jade B (FJB)-positive degenerative neurons per mm^3 in dentate hilar neurons, CA1 and CA3 neurons and PC neurons were $17\,545 \pm 2443$, $26\,318 \pm 1993$, $21\,358 \pm 2314$ and $24\,658 \pm 3698$, respectively, 3 days after SE (Supplementary Figure 1). In the PJ-34-treated group, the numbers of FJB-positive degenerative neurons per mm^3 in dentate hilar neurons, CA1 and CA3 neurons and PC neurons were $15\,432 \pm 1698$, $10\,841 \pm 1924$, 9818 ± 1152 and $2\,1742 \pm 4236$, respectively. In the DPQ-treated group, the numbers of FJB-positive degenerative neurons per mm^3 in dentate hilar neurons, CA1 and CA3 neurons and PC neurons were $16\,352 \pm 1785$, 9845 ± 1534, 8745 ± 1895 and $19\,857 \pm 5123$, respectively. These results revealed that PARP1 inhibitors attenuated SE-induced neuronal death in CA1 and CA3 neurons, but not in dentate hilar cells and PC neurons (Supplementary Figure 1, $P<0.05$ *versus* vehicle). Although PARP1 inhibitors themselves did not affect the number of GFAP-positive astrocytes in non-SE animals (data not shown), both PARP1 inhibitors effectively inhibited reactive astrogliosis in the CA1 region at 3 days after SE (Figures 6a and c). Following SE, however, PARP1 inhibitors induced astroglial death in the stratum lucidum of the CA3 region where astroglial loss was not observed in vehicle-treated group (Figures 6a and c, $P<0.05$ *versus* vehicle). Furthermore, PARP1 inhibitors deteriorated astroglial death in the molecular layer of the dentate gyrus following SE (Figures 6b and c, $P<0.05$ *versus* vehicle). PARP1 inhibitors did not affect SE-induced astroglial death in the PC (Figures 6a and c). Taken together, our findings indicate that PARP1 activation may play important roles in neuronal death and reactive astrogliosis within the CA1 and CA3 regions. However, PARP1 degradation/inactivation may involve in neuronal death in the PC and astroglial death in the molecular layer of the dentate gyrus following SE.

SE-induced PARP1 degradation and activation are independent of hemodynamics. To investigate whether the distinct microenvironment mediated by hemodynamics

Figure 1 PARP1 expression in the hippocampus following SE. (**a**) Western blot shows the gradual downregulation of full length of PARP1 protein without cleavage until 3 days after SE. At 1 and 4 weeks after SE, the expression of full length of PARP1 protein is increased as compared with 3 days after SE in the hippocampus. Cleaved PARP1 band is not observed in this region. (**b**) Quantification of full-length PARP1 protein levels (means ± S.E.M., $n=5$, respectively). *$P<0.05$ *versus* non-SE animals (one-way ANOVA test). (**c**) SE-induced PARP1 immunoreactivities in the hippocampus. Following SE, the number of PARP1-positive neurons is reduced in the CA1 and CA3 region, but not in dentate granule cell layer. In the molecular layer of the dentate gyrus, PARP1 expression is detected in some non-neuronal cells (arrows). Following SE, PARP1 expression in non-neuronal cells is undetectable in the molecular layer of the dentate gyrus. In contrast, PARP1 expression is increased in non-neuronal cells in the CA1–3 regions following SE (arrows). Panels 2–4 are the high-magnification photos of rectangles in panel 1. Bar = 400 μm (panel 1) and 50 μm (panels 2 and 3). (**d**) The changes in the number of PARP1-positive neurons in the hippocampus (means ± S.D., $n=5$, respectively). *$P<0.05$ *versus* non-SE animals (one-way ANOVA test)

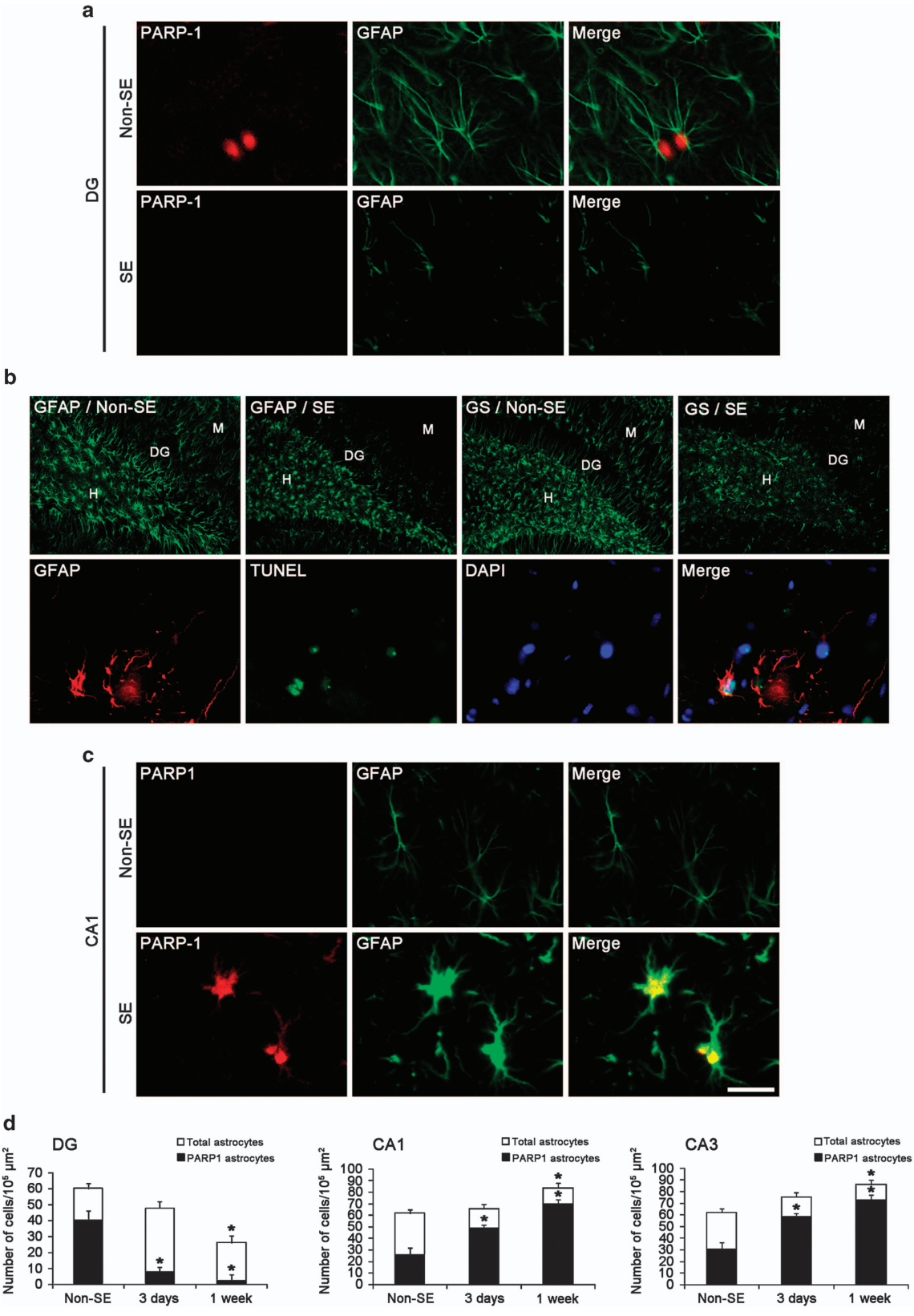
a
PARP-1
GFAP
Merge
Non-SE
SE
DG
b
GFAP / Non-SE
GFAP / SE
GS / Non-SE
GS / SE
M
DG
H
GFAP
TUNEL
DAPI
Merge
c
PARP1
GFAP
Merge
Non-SE
SE
CA1
PARP-1
d
DG
CA1
CA3
Total astrocytes
PARP1 astrocytes
Number of cells/10⁵ μm²
Non-SE
3 days
1 week

results in the regional-specific PARP1 degradation and activation following SE, we applied *ex vivo* model (acute brain slices) to rule out the hemodynamic effects. As compared with normal artificial cerebrospinal fluid (ACSF), ACSF + pilocarpine (PILO) decreased the number of PARP1-positive astrocytes within the molecular layer of the dentate gyrus without reduction in the number of GFAP-positive astrocytes (Figure 7 and Supplementary Figure 2a, $P<0.05$ *versus* normal ACSF). In contrast, ACSF + PILO increased the number of PARP1-positive astrocytes within the CA1 and CA3 fields (Figure 7 and Supplementary Figure 2a, $P<0.05$ *versus* normal ACSF). In the PC, ACSF + PILO reduced the numbers of GFAP-positive astrocytes and PARP1-positive neurons (Figure 7 and Supplementary Figure 2a, $P<0.05$ *versus* normal ACSF). ACSF + PILO did not induce PARP1 expression in microglia (data not shown). Western blot study also showed that ACSF + PILO resulted in upregulation of full length of PARP1 expression in the hippocampus. However, it reduced PARP1 expression in the PC (Supplementary Figures 2b and c, $P<0.05$). Similar to the *in vivo* model, cleaved PARP1 fragments were not observed in the hippocampus or the PC (Supplementary Figures 2b and c).

ACSF + PILO did not induce neuronal death in the hippocampus and the PC (Figure 8a). In the hippocampal neurons, ACSF + PILO resulted in PAR induction without alteration in PARP1 expression (Supplementary Figure 3). In PC neurons, ACSF + PILO reduced PARP1 expression accompanied by PAR induction (Supplementary Figure 3). ACSF + PILO reduced the number of GFAP-positive astrocytes in the PC, but not in the molecular layer of the dentate gyrus (Figures 8a and b). ACSF + PILO did not induce PAR immunoreactivity in astrocytes (data not shown). As compared with ACSF + PILO, PARP1 inhibitors reduced the number of GFAP-positive astrocytes in the stratum lucidum of the CA3 region, but did not affect astroglial loss in the PC and the molecular layer of the dentate gyrus (Figures 8a and b). These findings indicate that SE may change the profiles of PARP1 expression in neurons and astrocytes in a hemodynamic-independent manner.

Discussion

PARP1 activation involves SE-induced neuronal death in CA1 and CA3 neurons. Although PARP1 promotes cell survival after DNA damage,[26] excessive PARP1 activation causes cell death because of energy failure and mitochondrial dysfunction.[1,2,27–29] Thus, it is generally accepted that PARP1 inhibition prevents neuronal death through preservation of the energy-dependent cellular function.[5,30] The vulnerability of neurons to insults is not uniform, but is heterogeneous among the various brain regions. Briefly, dentate granule cells are remarkably resistant to neuronal damage caused by most insults.[31–33] Conversely, the CA1 and CA3 neurons, hilar neurons and PC neurons are extremely vulnerable to various harmful stimuli.[31–34] In the present study, SE-induced neuronal death was not detected in dentate granule cells, but in CA1 and CA3 neurons and PC neurons. Furthermore, PARP1 inhibitors effectively attenuated SE-induced neuronal death in CA1 and CA3 neurons, but not in PC neurons. Therefore, these findings indicate that PARP1 activation may induce CA1 and CA3 neuronal death following SE. However, PC neurons may be damaged independently of PARP1 activation.

PARP1 degradation induces PC neuronal death in a hemodynamic-independent manner following SE. In the present study, most of CA1 and CA3 neurons showed PAR synthesis *in vivo* at 12 h after SE, whereas a few PC exhibited it. We hypothesized that these differential responses of PARP1 to SE would be most likely because of the distinctive hemodynamic characteristics between PC and the hippocampus *in vivo*. To confirm this hypothesis, we performed *ex vivo* study. Similar to *in vivo* model, *ex vivo* model showed PAR induction in most of CA1 and CA3 neurons without alteration in PARP1 expression. However, PC neurons showed less PAR induction and PARP1 expression than those in CA1 and CA3 neurons. These findings indicate that PARP1 degradation may involve SE-induced neuronal death in PC neurons unlike hippocampal neurons, and that the regional-specific pattern of PARP1 degradation may be hemodynamic-independent neuronal responses to SE *per se*.

PARP1 degradation results in SE-induced astroglial death. Since Schmidt-Kastner and Ingvar[35,36] described regional-specific astroglial damage in the brain after SE, increasing evidence supports that SE leads to devastating astroglial death that is characterized by regional-specific patterns.[19,24,25] However, the molecular events underlying the occurrence of regional-specific astroglial death are unclear. In the present study, PARP1 degradation was observed in astrocytes within the molecular layer of the dentate gyrus showing astroglial loss induced by SE. PARP1 inhibitors deteriorated SE-induced astroglial death in the molecular layer of the dentate gyrus. Following SE, PARP1 inhibitors also induced astroglial death in the stratum lucidum of the CA3 region where astroglial loss was not observed in vehicle-treated animals. In *ex vivo* model, PARP1 inhibitors similarly induced astroglial death in the CA3 region. As in the

Figure 2 Astroglial PARP1 expression in the hippocampus following SE. (**a**) Astroglial PARP1 degradation in the molecular layer of the dentate gyrus following SE. In the molecular layer of the dentate gyrus, PARP1 expression is detected in astrocytes. Following SE, PARP1 expression in astrocytes is undetectable in this region accompanied by downregulation of GFAP expression. Bar = 12.5 μm. (**b**) Astroglial death induced by SE. Following SE, both GFAP and GS expression are reduced in the molecular layer of the dentate gyrus. M, molecular layer; DG, dentate granule cell layer; H, hilus. Bar = 50 μm. In addition, TUNEL-positive astrocytes show downregulation of GFAP expression. Bar = 12.5 μm. (**c**) Astroglial PARP1 induction in the stratum radiatum of the CA1 region following SE. In non-SE animals, few astrocytes show PARP1 immunoreactivity in the CA1 region. Following SE, reactive astrocytes contain PARP1 immunoreactivity. Bar = 12.5 μm. (**d**) The changes in the number of total astrocytes and PARP1-positive astrocytes in the hippocampus following SE. In the molecular layer of the dentate gyrus (DG), the fraction of PARP1-positive astrocytes in total astrocytes is reduced following SE. In the CA1 and CA3 regions, the numbers of total astrocytes and the fraction of PARP1-positive astrocytes in total astrocytes are gradually increased following SE (means ± S.D., $n=5$, respectively). *$P<0.05$ *versus* non-SE animals (one-way ANOVA test)

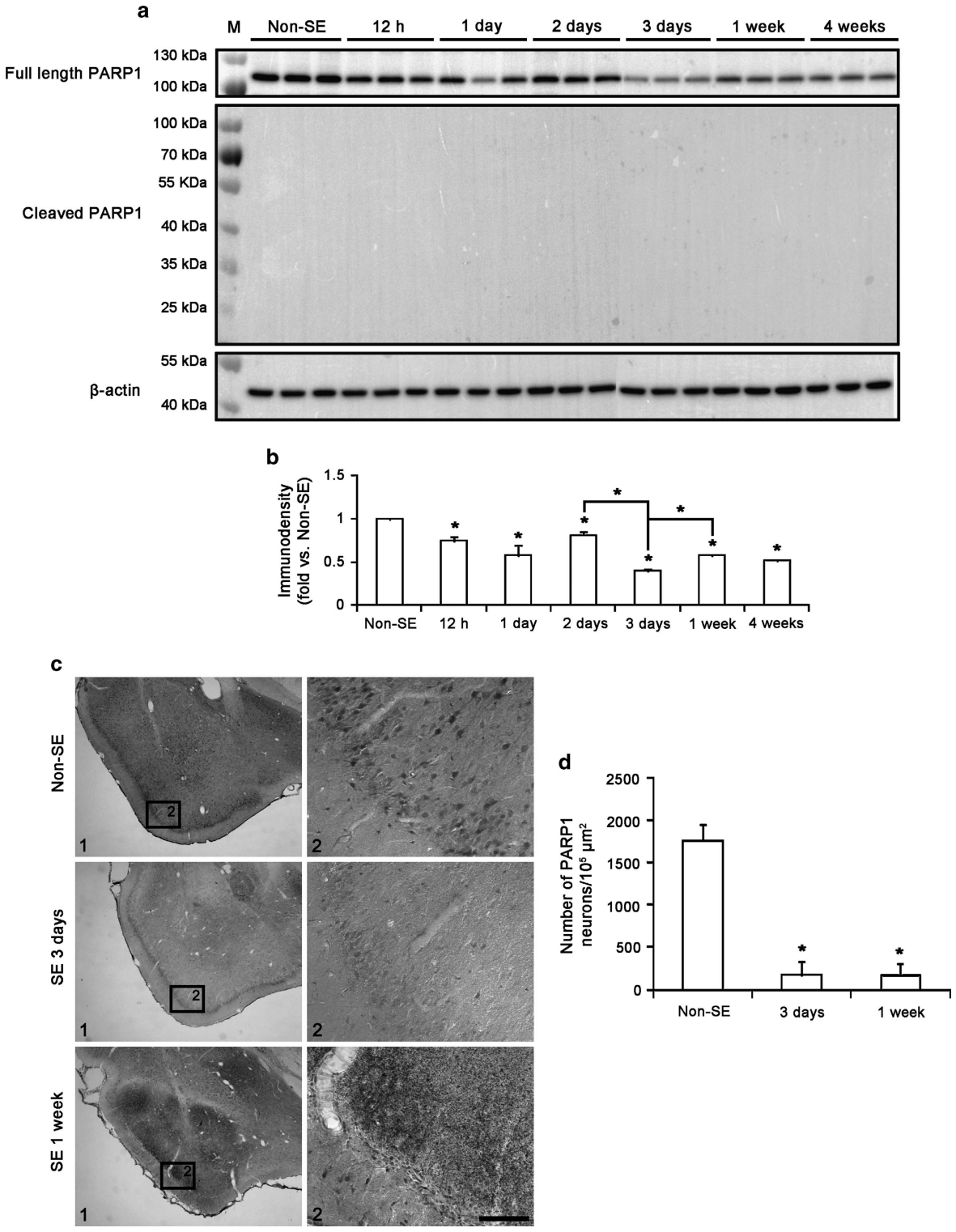

Figure 3 PARP1 expression in the PC following SE. (**a**) Western blot shows the gradual downregulation of full length of PARP1 protein without cleavage until 3 days after SE. At 1 to 4 weeks after SE, the expression of full length of PARP1 protein is increased as compared with 3 days after SE in the PC. Cleaved PARP1 band is not observed in this region. (**b**) Quantification of full-length PARP1 protein levels (means ± S.E.M., $n = 5$, respectively). *$P < 0.05$ *versus* non-SE animals (one-way ANOVA test). (**c**) SE-induced PARP1 immunoreactivities in the PC. Following SE, the number of PARP1-positive neurons is reduced in the PC. However, PARP1 expression is increased in non-neuronal cells in the PC. Panel 2 shows high-magnification photos of rectangles in panel 1. Bar = 400 μm (panel 1) and 50 μm (panel 2). (**d**) The changes in the number of PARP1-positive neurons in the PC (means ± S.D., $n = 5$, respectively). *$P < 0.05$ *versus* non-SE animals (one-way ANOVA test)

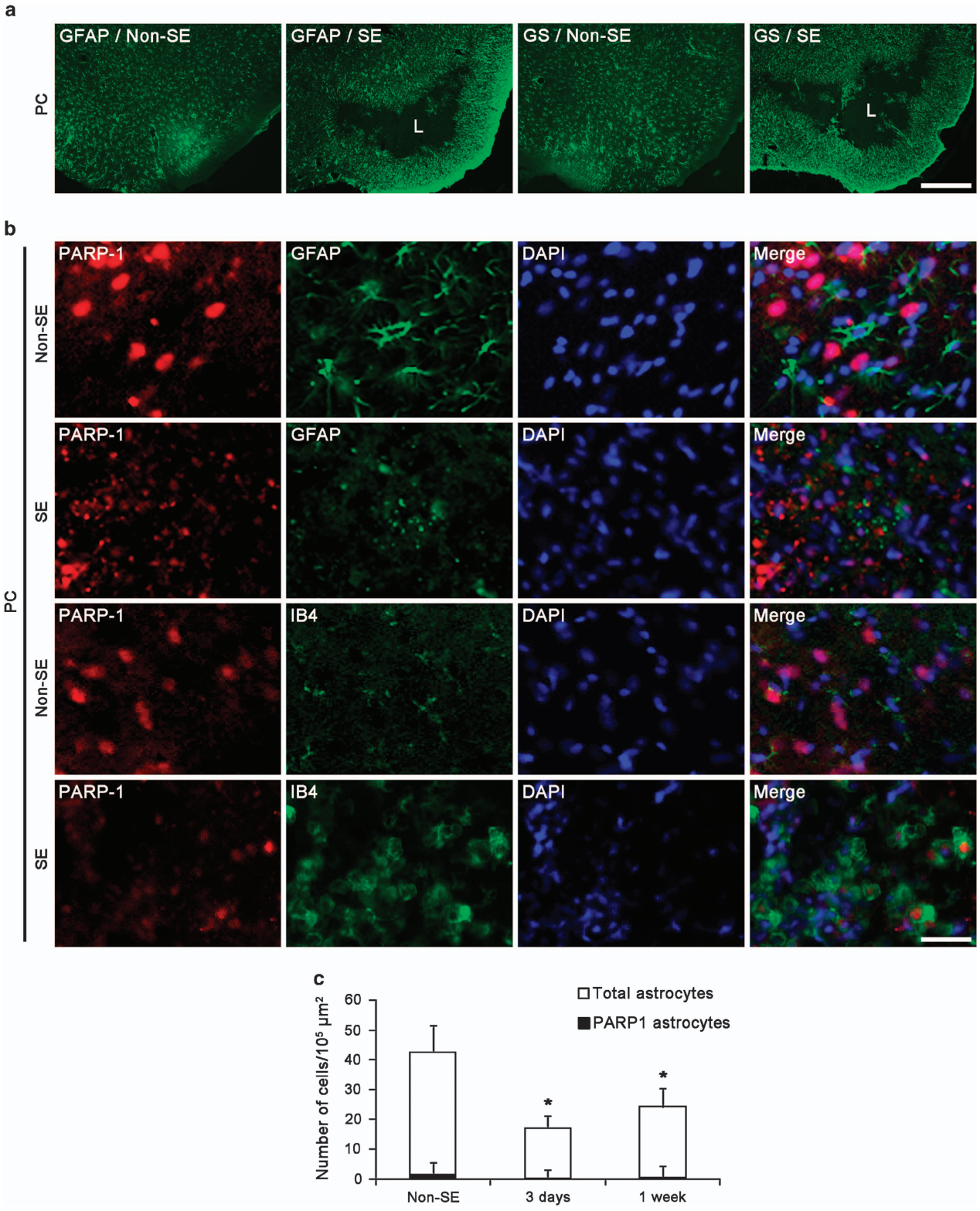

Figure 4 Astroglial death and microglial PARP1 induction in the PC following SE. (**a**) Astroglial death induced by SE. Both GFAP and GS expression are reduced in the PC. Astroglial depleted lesion (L) is surrounded by reactive astrocytes. Bar = 200 μm. (**b**) Double immunofluorescent images for PARP1 and GFAP/IB4 in the PC. In non-SE animals, PARP1 expression is detected only in PC neurons. Following SE, PARP1 degradation and GFAP-positive astroglial loss are observed in the PC. In addition, IB4-positive microglia show PARP1 immunoreactivity. Bar = 12.5 μm. (**c**) The changes in the number of total astrocytes and PARP1-positive astrocytes in the hippocampus following SE. The number of total astrocytes is reduced at 3 days to 1 week after SE, whereas the fraction of PARP1-positive astrocytes in total astrocytes is unaltered (means ± S.D., $n = 5$, respectively). *$P < 0.05$ *versus* non-SE animals (one-way ANOVA test)

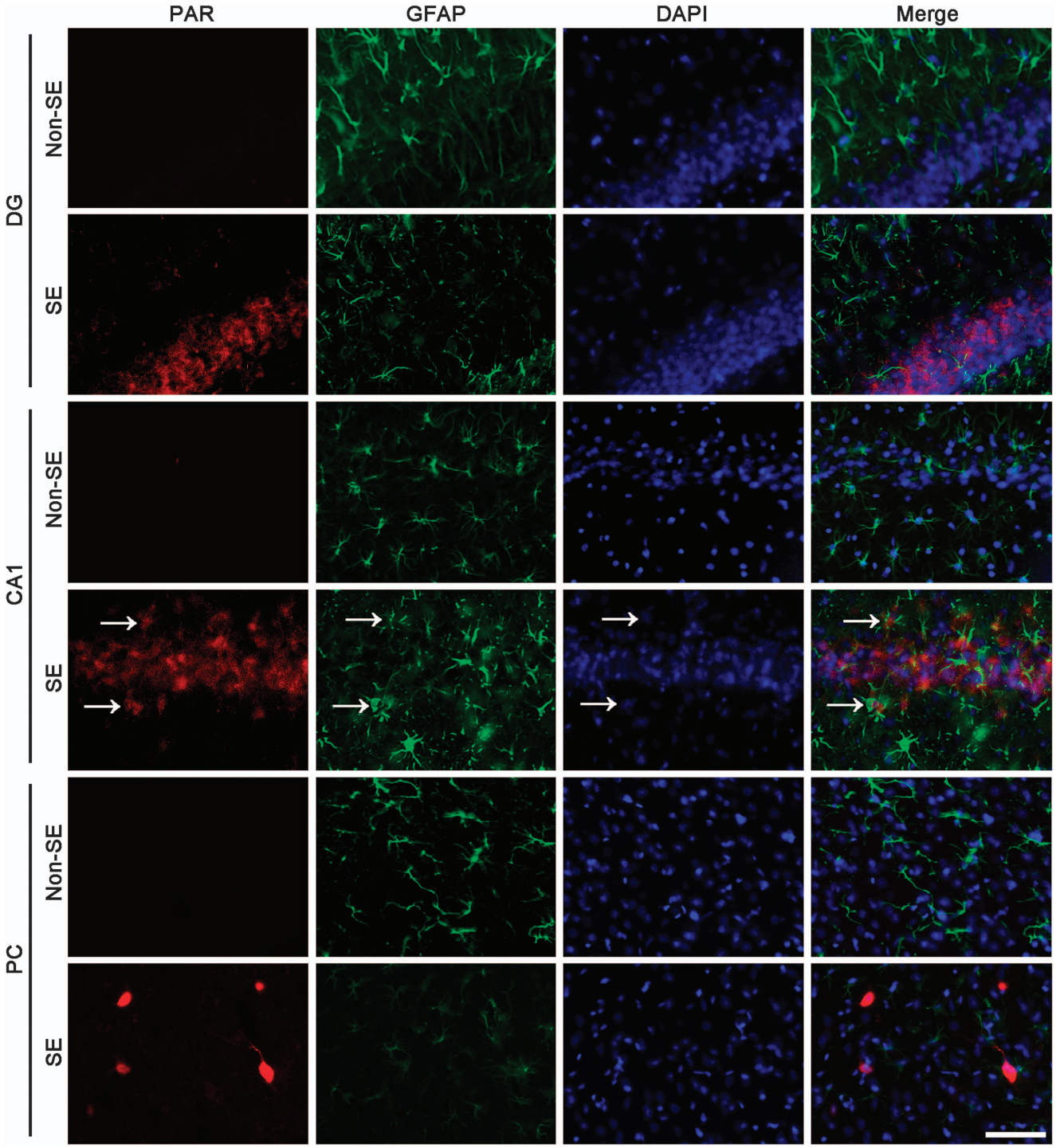

Figure 5 SE-induced PARP activation (PAR synthesis) in the hippocampus and the PC *in vivo*. In non-SE animals, PAR immunoreactivity is rarely observed in the hippocampus and the PC. At 12 h after SE, PAR is detected in the CA1–3 neurons, dentate granule cells, hilar neurons and PC neurons. PAR immunoreactivity is also observed in some astrocytes in the CA1 region (arrows). Bar = 25 μm

case of neurons, the present data suggest that regional-specific astroglial PARP1 responses to SE may be independent of hemodynamics. In the present study, massive astroglial-deleted lesion was also observed in the PC where astroglial PARP1 expression was undetected before/after SE. In addition, PARP1 inhibitors did not affect astroglial death in the PC unlike the molecular layer of the dentate gyrus. Similarly, we have reported that P2 $\times$ 7 receptor antagonists could not prevent astroglial death in the PC, whereas they effectively attenuated astroglial loss in the molecular layer of the dentate gyrus following SE.[23] Although further studies are needed to elucidate the mechanism of

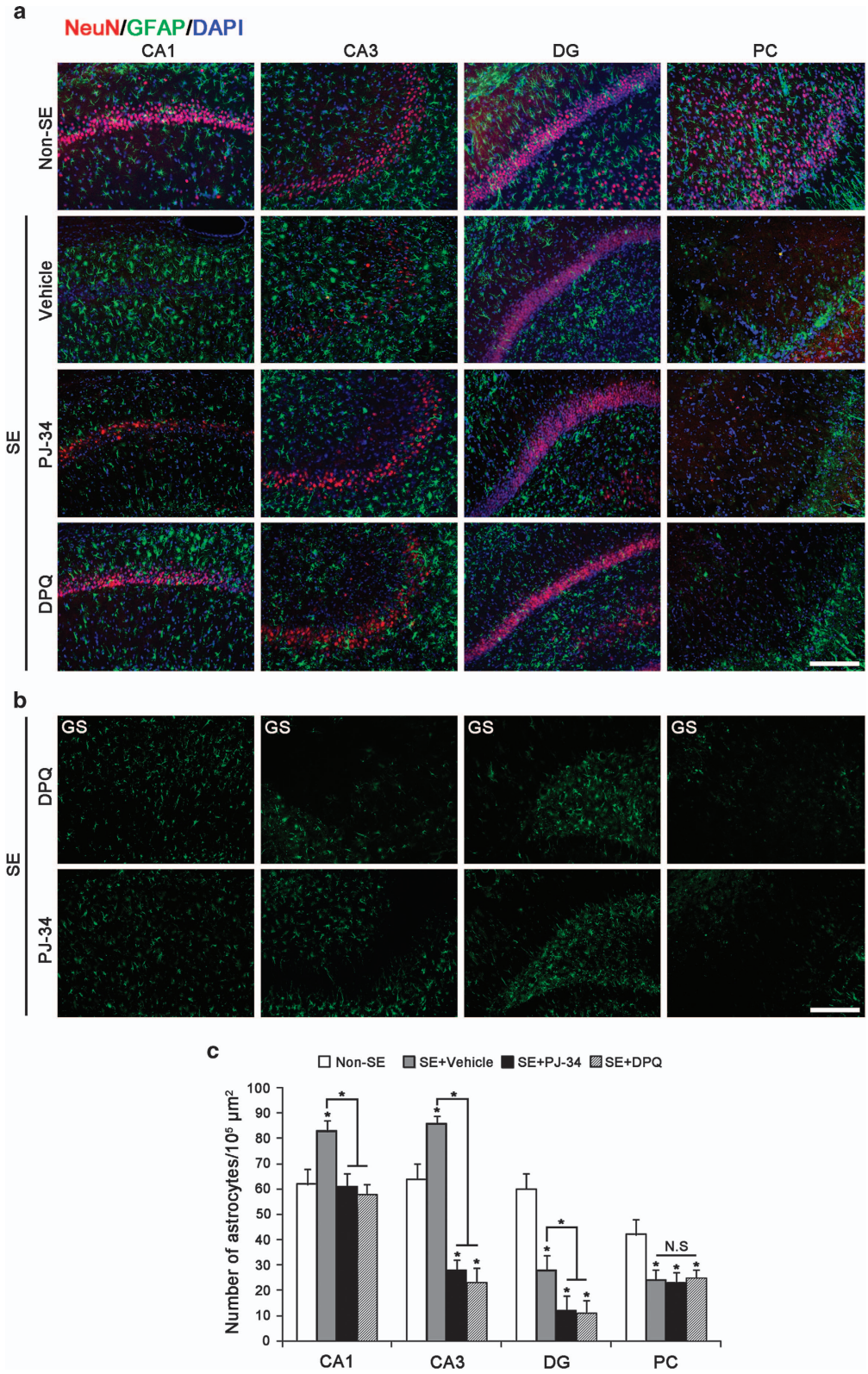

Figure 6 The effect of PARP1 inhibitors (PJ-34 and DPQ) on SE-induced astroglial responses in the hippocampus and the PC *in vivo*. (**a**) In the CA1 region, both PARP1 inhibitors inhibit SE-induced reactive gliosis to the extent of non-SE level at 3 days after SE. In the CA3 region, both PARP1 inhibitors induce astroglial death in the stratum lucidum following SE. In the DG region, both PARP1 inhibitors aggravate astroglial loss in the molecular layer of the dentate gyrus following SE. In the PC, PARP1 inhibitors do not affect SE-induced astroglial death at 3 days after SE. Bar = 50 μm. (**b**) The effect of PARP1 inhibitors (DPQ and PJ-34) on GS expression is similar to those on GFAP expression in the hippocampus and the PC *in vivo*. Bar = 50 μm. (**c**) Quantification of the number of astrocytes following SE (means ± S.D., $n = 5$, respectively). *$P < 0.05$ *versus* non-SE animals (one-way ANOVA test)

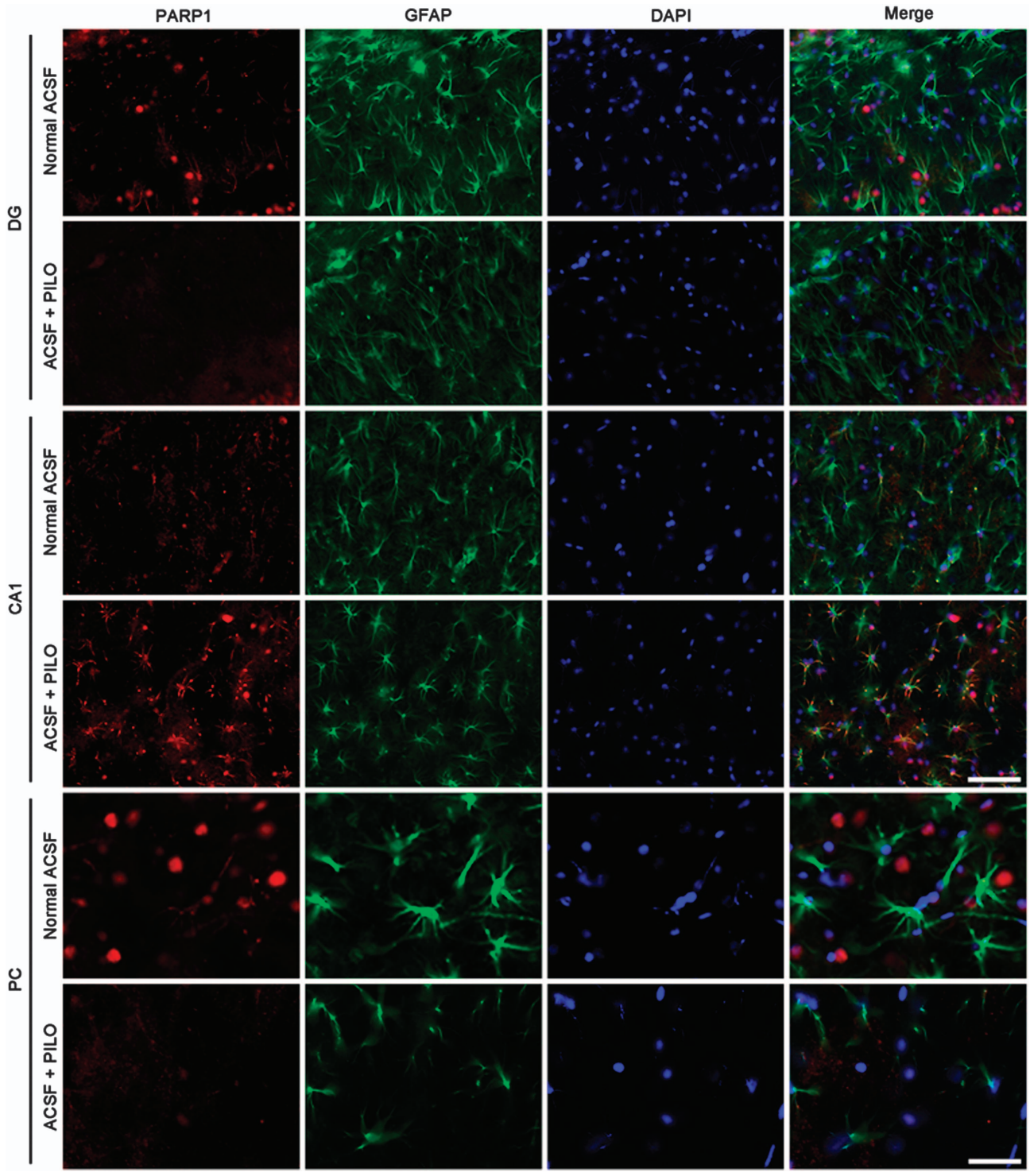

Figure 7 The effect of PILO on PARP1 and GFAP expression *ex vivo*. In the DG, ACSF + PILO decreased PARP1 expression in astrocytes, but increased it in astrocytes in the CA1 region. In the PC, ACSF + PILO reduced PARP1 expression and the number of GFAP-positive astrocytes. Bar = 25 μm (DG and CA1) and 12.5 μm (PC)

SE-induced astroglial death in the PC, it is likely that the distinct mechanisms involve astroglial death in the different regions. Taken together, our findings indicate that PARP1 degradation/inactivation may be one of the determining factors in regional-specific astroglial death in response to SE insults.

PARP1 activation induces regional-specific reactive gliosis induced by SE. Reactive gliosis is characterized by the proliferation of microglia and astrocytes as well as by astroglial hypertrophy following injury in the brain.[37,38] PARP1 expression/activation in glial cells allows the function of transcription factors such as nuclear factor-κB, activator

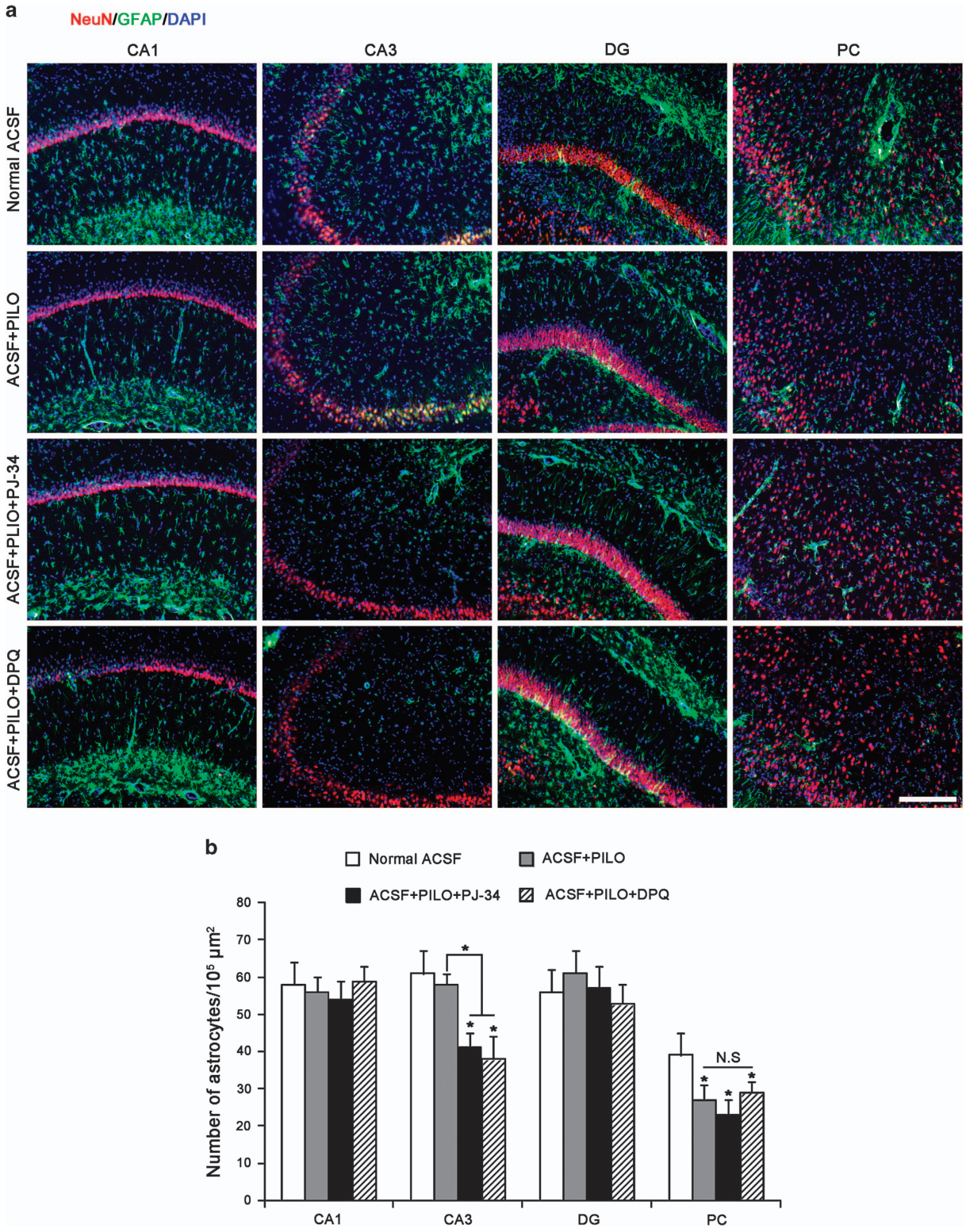

Figure 8 The effect of PARP1 inhibitors (PJ-34 and DPQ) on PILO-induced astroglial responses in the hippocampus and the PC *ex vivo*. (**a**) ACSF + PILO did not induce neuronal death in the CA1–3 regions and the dentate gyrus. Both PARP1 inhibitors induced astroglial loss in the stratum lucidum of the CA3 region. In the PC region, ACSF + PILO induced astroglial loss. Both PARP1 inhibitors are ineffective to astroglial death induced by ACSF + PILO. Bar = 50 μm. (**b**) Quantification of the number of astrocytes (means ± S.D., $n = 5$, respectively). *$P < 0.05$ *versus* normal ACSF (one-way ANOVA test)

protein-1 and cAMP-response element binding protein that control cell proliferation and inflammatory responses.[39–44] In the present study, astrocytes in the CA1–3 region showed PAPR1 and PAR inductions following SE. The *ex vivo* model also showed the astroglial PARP1 induction, although PAR immunoreactivity was undetectable. Furthermore, PARP1 inhibitors effectively inhibited reactive astrogliosis in the CA1 region. As reactive astrogliosis occurs rather early after insult, even before any obvious neuronal damage,[45] our findings indicate that PARP1 induction/activation may influence the early steps of the astroglial activation. PARP1 also expresses in activated microglia/infiltrated monocytes, and plays an important role in the regulation of neuroinflammatory responses.[46] In previous study, we reported that resident microglia are replaced by blood-derived monocytes in PC after SE.[24] In the present study, IB4-positive cells in non-SE animals had no PARP1 expression in the PC *in vivo*. Following SE, IB4-positive cells had strong PARP1 expression in the PC. Therefore, our findings indicate that PARP1 induction may play an important role in reactive microgliosis and in the activation of infiltrated monocytes following SE.

In conclusion, we provide novel evidence that PARP1 activation/degradation shows regional- and cellular-specific patterns in hemodynamic-independent manners. To the best of our knowledge, the present study proposes for the first time the role of PARP1 in neuron–astroglial death and reactive gliosis. Therefore, we suggest that the selective modulation of PARP1 activation/degradation may be a considerable strategy for therapy in various neurological diseases.

Materials and Methods

Experimental animals. This study utilized the progeny of Sprague-Dawley (SD) rats (male, 9–11 weeks old) obtained from Experimental Animal Center, Hallym University, Chunchon, South Korea. The animals were provided with a commercial diet and water *ad libitum* under controlled temperature, humidity and lighting conditions (22 ± 2 °C, 55 ± 5% and a 12 : 12 light/dark cycle with lights). Procedures involving animals and their care were conducted in accord with our institutional guidelines that comply with NIH Guide for the Care and Use of Laboratory Animals (NIH Publications No. 80–23, 1996). In addition, we have made all efforts to minimize the number of animals used and their suffering.

Intracerebroventricular drug infusion. Rats were divided into three groups: vehicle (saline)-treated group, PJ-34-treated group (PARP inhibitor VIII, 3 μM, Merck, Darmstadt, Germany) and DPQ-treated group (PARP inhibitor III, 5 μM, Merck) ($n = 30$, respectively). The dosage of each compound was determined as the highest dose that did not affect seizure threshold in the preliminary study. Animals were anesthetized (Zolretil, 50 mg/kg, i.m., Virbac Laboratories, Carros, France) and placed in stereotaxic frames. For the osmotic pump implantation, holes were drilled through the skull for introducing a brain infusion kit 1 (Alzet, Palo Alto, CA, USA) into the right lateral ventricle (1 mm posterior; 1.5 mm lateral; -3.5 mm depth; flat skull position with bregma as reference), according to the atlas of G. Paxinos and C. Watson, *The rat brain in stereotaxic coordinates* (3rd ed.), Academic Press, San Diego (1997).[47] The infusion kit was sealed with dental cement and connected to an osmotic pump (1007D, Alzet). The pump was placed in a subcutaneous pocket in the dorsal region. Animals received 0.5 μl/h of vehicle or compound for 1 week.[21,25]

Seizure induction. At 3 days after surgery, rats were treated with PILO (380 mg/kg, i.p.) 20 min after injection of methylscopolamine (5 mg/kg, i.p.). Approximately 80% of PILO-treated rats showed acute behavioral features of SE (including akinesia, facial automatisms, limbic seizures consisting of forelimb clonus with rearing, salivation, masticatory jaw movements and falling). Diazepam (10 mg/kg, i.p.) was administered 2 h after onset of SE and repeated, as needed. Age-matched animals were used as non-SE-experienced controls (non-SE animals, $n = 30$). Non-SE animals received saline in place of PILO. At designated time courses, animals were used for immunohistochemistry and western blot.

Acute brain slices. Animals ($n = 15$) were anesthetized with urethane anesthesia (1.5 g/kg, i.p.) and decapitated. Brains were rapidly removed and placed in ice-cold cutting solution (composition in mM: KCl 3, NaH_2PO_4 1.25, $MgSO_4$ 6, $NaHCO_3$ 26, $CaCl_2$ 0.2, glucose 10 and sucrose 220). Coronal sections (300 μm thickness) were cut on a Vibratome (Campden Instruments Limited, Loughborough, UK) and slices were subsequently transferred to oxygenated ACSF (composition in mM: NaCl 124, KCl 2.5, $NaHCO_3$ 26, KH_2PO_4 1.25, $MgSO_4$ 2, $CaCl_2$ 2.5, glucose 10 and sucrose 4, pH 7.4, bubbled with 95% O_2 and 5% CO_2) at room temperature.[48] Cutting solution was 300–305 mOsm/l. After warming to 34 °C for 30 min, the ACSF was exchanged again, and slices were then held at room temperature. Individual slices were then transferred to a chamber and perfused with oxygenated ACSF at 2 ml/min.[48] Some slices were treated with PJ-34 (1 μM) or DPQ (5 μM) in ACSF. After 10 min of incubation, PILO (5 mM) was added in each chamber for 2 h. After culture, slices were fixed with 4% paraformaldehyde in 0.1 M phosphate buffer (PB, pH 7.4) for immunohistochemical study or homogenated for western blot.

Tissue processing. Animals were perfused transcardially with phosphate-buffered saline (PBS) followed by 4% paraformaldehyde in 0.1 M PB (pH 7.4) under urethane anesthesia (1.5 g/kg, i.p.). The brains were removed, and postfixed in the same fixative for 4 h. The brain tissues were cryoprotected by infiltration with 30% sucrose overnight. Thereafter, the entire hippocampus was frozen and sectioned with a cryostat at 30 μm and consecutive sections were contained in six-well plates containing PBS. For stereological study, every sixth section in the series throughout the entire hippocampus was used in some animals.

FJB staining. FJB staining was used to identify degenerating neurons. Briefly, sections were rinsed in distilled water, and mounted onto gelatin-coated slides and then dried on a slide warmer. The slides were immersed in 100% ethanol for 3 min, followed by 70% ethanol for 2 min and distilled water for 2 min. The slides were then transferred to 0.06% potassium permanganate for 15 min and gently agitated. After rinsing in distilled water for 2 min, the slides were incubated for 30 min in 0.001% FJB (Histo-Chem Inc., Jefferson, AR, USA), freshly prepared by adding 20 ml of a 0.01% stock FJB solution to 180 ml of 0.1% acetic acid, with gentle shaking in the dark. After rinsing for 1 min in each of three changes of distilled water, the slides were dried, dehydrated in xylene and coverslipped with DPX. For stereological study, every sixth section in the series throughout the entire hippocampus and PC were used (see below).

Immunohistochemistry. The sections were first incubated with 3% bovine serum albumin in PBS for 30 min at room temperature. They were then incubated with rabbit anti-PARP1 IgG (diluted 1 : 500; Abnova, Taipei, Taiwan) in PBS containing 0.3% Triton X-100 and 2% normal chicken serum overnight at room temperature. After washing three times for 10 min with PBS, sections were incubated sequentially with the secondary antibody and ABC complex (Vector Laboratories Inc., Carros, France) and diluted 1 : 200 in the same solution as the primary antiserum. Between incubations, tissues were washed with PBS three times for 10 min each. The sections were visualized using 3,3′-diaminobenzidine in 0.1 M Tris buffer and mounted on gelatin-coated slides. Immunoreactions were observed using an Axio Scope microscope (Carl Zeiss, Inc., Göttingen, Germany). To establish the specificity of the immunostaining, a negative control test was carried out with preimmune serum instead of the primary antibody. No immunoreactivity was observed for the negative control in any structures. All experimental procedures in this study were performed under the same conditions and in parallel.

Immunofluorescence staining. Brain tissues were incubated with mixtures of mouse anti-GFAP IgG (diluted 1 : 100; Millipore, Bedford, MA, USA)/rabbit anti-PARP1 IgG (diluted 1 : 100; Abnova), rabbit anti-PARP1 IgG (diluted 1 : 100; Abnova)/IB4 lectin (diluted 1 : 200, Vector, Burlingame, CA, USA), rabbit anti-GFAP IgG (diluted 1 : 200; Promega, Madison, WI, USA)/mouse anti-PAR IgG (diluted 1 : 100; Trevigen, Gaithersburg, MD, USA), rabbit anti-GFAP IgG (diluted 1 : 500; Promega)/mouse anti-NeuN IgG (diluted 1 : 500; Abnova) or mouse anti-PAR IgG (diluted 1 : 100; Trevigen)/rabbit anti-PARP1 IgG (diluted 1 : 100; Abnova) in PBS containing 0.3% Triton X-100 and 2% normal chicken serum overnight at room temperature. Some brain sections were reacted with only mouse anti-GS IgG (diluted 1 : 100; Millipore). After washing three times for 10 min with

PBS, sections were also incubated in a mixture of FITC- and Cy3-conjugated secondary antisera (Amersham, Piscataway, NJ, USA, 1 : 200) for 1 h at room temperature. Sections were mounted in Vectashield mounting media with/without DAPI (Vector). Images were captured using an Axiocam HRc camera and Axio Vision 3.1 software or confocal laser scanning microscope (LSM 510 META, Carl Zeiss, Inc.). Figures were mounted with Adobe PhotoShop 7.0 (San Jose, CA, USA). Manipulation of the images was restricted to threshold and brightness adjustments to the whole image.

TUNEL staining. TUNEL staining was performed with the TUNEL apoptosis detection kit (Cat.# 17-141, Merck Millipore, Bedford, MA, USA) according to the manufacturer's instructions. Following TUNEL reaction, GFAP immunofluorescence staining was performed. For nuclei counterstaining, we used Vectashield mounting medium with DAPI (Vector). All images were captured using an Axiocam HRc camera and Axio Vision 3.1 software.

Cell counts. For quantification of immunohistochemical data, cells in 2–4 regions (1×10^5 μm^2) from each section were counted on 20 $\times$ images. Results are presented as means $\pm$ S.D. of 15–24 regions from 5 animals. For quantification of GFAP/PARP1 double immunofluorescence, the number of GFAP-positive cells showing PARP1 induction was actually counted within the sampled images. All immunoreactive cells were counted regardless of the intensity of labeling. Cell counts were performed by two different investigators who were blind to the classification of tissues.

Western blot. Aliquots containing 20 μg total protein were boiled in a loading buffer containing 150 mM Tris (pH 6.8), 300 mM DTT, 6% sodium dodecyl sulfate (SDS), 0.3% bromophenol blue and 30% glycerol. Each aliquot was loaded into a 10% polyacrylamide gel. After electrophoresis, gels were transferred to nitrocellulose transfer membranes (Schleicher and Schuell BioScience Inc., Keene, NH, USA). To reduce background staining, the filters were incubated with 5% nonfat dry milk in TBS containing 0.1% Tween-20 for 45 min, followed by incubation with rabbit anti-PARP1 (1 : 500; Abnova), cleaved PARP1 (1 : 500; Biovision, Mountain View, CA, USA) or mouse anti-β-actin (1 : 5000; Sigma, St. Louis, MO, USA) and subsequently with an HRP-conjugated secondary antibody. Western blotting was performed with an ECL Western Blotting Detection Kit (Amersham). Intensity measurements were represented as the mean gray-scale value on a 256 gray-level scale. Results are presented as means $\pm$ S.E.M.[21]

Data analysis. All data obtained from the quantitative measurements were analyzed using Student's *t*-test or one-way ANOVA to determine statistical significance. Bonferroni's test was used for *post hoc* comparisons. A *P*-value of < 0.05 was considered statistically significant.[20,21,49]

Conflict of Interest

The authors declare no conflict of interest.

Acknowledgements. This work was supported by the National Research Foundation of Korea (NRF) grant funded by the Korea government (MEST) (no. 2012R1A2A1A01001775 and 2013R1A6A3A04058272).

1. Berger NA. Poly(ADP-ribose) in the cellular response to DNA damage. *Radiat Res* 1985; **101**: 4–15.
2. Ha HC, Snyder SH. Poly(ADP-ribose) polymerase is a mediator of necrotic cell death by ATP depletion. *Proc Natl Acad Sci USA* 1999; **96**: 13978–13982.
3. Szabó C, Dawson VL. Role of poly(ADP-ribose) synthetase in inflammation and ischaemia-reperfusion. *Trends Pharmacol Sci* 1998; **19**: 287–298.
4. Virág L, Szabó C. The therapeutic potential of poly(ADP-ribose) polymerase inhibitors. *Pharmacol Rev* 2002; **54**: 375–429.
5. Ying W, Chen Y, Alano CC, Swanson RA. Tricarboxylic acid cycle substrates prevent PARP-mediated death of neurons and astrocytes. *J Cereb Blood Flow Metab* 2002; **22**: 774–779.
6. Zhang J, Dawson VL, Dawson TM, Snyder SH. Nitric oxide activation of poly(ADP-ribose) synthetase in neurotoxicity. *Science* 1994; **263**: 687–689.
7. Kaufmann SH, Desnoyers S, Ottaviano Y, Davidson NE, Poirier GG. Specific proteolytic cleavage of poly(ADP-ribose) polymerase: an early marker of chemotherapy-induced apoptosis. *Cancer Res* 1993; **53**: 3976–3985.
8. Lazebnik YA, Kaufmann SH, Desnoyers S, Poirier GG, Earnshaw WC. Cleavage of poly(ADP-ribose) polymerase by a proteinase with properties like ICE. *Nature* 1994; **371**: 346–347.
9. Matsushima S, Okita N, Oku M, Nagai W, Kobayashi M, Higami Y. An Mdm2 antagonist, Nutlin-3a, induces p53-dependent and proteasome-mediated poly(ADP-ribose) polymerase1 degradation in mouse fibroblasts. *Biochem Biophys Res Commun* 2011; **407**: 557–561.
10. Nagai W, Okita N, Matsumoto H, Okado H, Oku M, Higami Y. Reversible induction of PARP1 degradation by p53-inducible cis-imidazoline compounds. *Biochem Biophys Res Commun* 2012; **421**: 15–19.
11. Guillouf C, Vit JP, Rosselli F. Loss of the Fanconi anemia group C protein activity results in an inability to activate caspase-3 after ionizing radiation. *Biochimie* 2000; **82**: 51–58.
12. Wang T, Simbulan-Rosenthal CM, Smulson ME, Chock PB, Yang DC. Polyubiquitylation of PARP-1 through ubiquitin K48 is modulated by activated DNA, NAD +, and dipeptides. *J Cell Biochem* 2008; **104**: 318–328.
13. DeLorenzo RJ, Pellock JM, Towne AR, Boggs JG. Epidemiology of status epilepticus. *J Clin Neurophysiol* 1995; **12**: 316–325.
14. Fujikawa DG. Neuroprotective effect of ketamine administered after status epilepticus onset. *Epilepsia* 1995; **36**: 186–195.
15. Rice AC, DeLorenzo RJ. NMDA receptor activation during status epilepticus is required for the development of epilepsy. *Brain Res* 1998; **782**: 240–247.
16. Dawson VL, Dawson TM. Nitric oxide neurotoxicity. *J Chem Neuroanat* 1996; **10**: 179–190.
17. Bordey A, Sontheimer H. Properties of human glial cells associated with epileptic seizure foci. *Epilepsy Res* 1998; **32**: 286–303.
18. Mathern GW, Pretorius JK, Kornblum HI, Mendoza D, Lozada A, Leite JP *et al.* Altered hippocampal kainate-receptor mRNA levels in temporal lobe epilepsy patients. *Neurobiol Dis* 1998; **5**: 151–176.
19. Kang TC, Kim DS, Kwak SE, Kim JE, Won MH, Kim DW *et al.* Epileptogenic roles of astroglial death and regeneration in the dentate gyrus of experimental temporal lobe epilepsy. *Glia* 2006; **54**: 258–271.
20. Kim DS, Kim JE, Kwak SE, Choi KC, Kim DW, Kwon OS *et al.* Spatiotemporal characteristics of astroglial death in the rat hippocampo-entorhinal complex following pilocarpine-induced status epilepticus. *J Comp Neurol* 2008; **511**: 581–598.
21. Kim JE, Kang TC. The P2X7 receptor-pannexin-1 complex decreases muscarinic acetylcholine receptor-mediated seizure susceptibility in mice. *J Clin Invest* 2011; **121**: 2037–2047.
22. Ryu HJ, Kim JE, Yeo SI, Kim DW, Kwon OS, Choi SY *et al.* F-actin depolymerization accelerates clasmatodendrosis via activation of lysosome-derived autophagic astroglial death. *Brain Res Bull* 2011a; **85**: 368–373.
23. Ryu HJ, Kim JE, Yeo SI, Kang TC. p65/RelA-Ser529 NF-κB subunit phosphorylation induces autophagic astroglial death (Clasmatodendrosis) following status epilepticus. *Cell Mol Neurobiol* 2011b; **31**: 1071–1078.
24. Kim JE, Yeo SI, Ryu HJ, Kim MJ, Kim DS, Jo SM *et al.* Astroglial loss and edema formation in the rat piriform cortex and hippocampus following pilocarpine-induced status epilepticus. *J Comp Neurol* 2010; **518**: 4612–4628.
25. Kim JE, Ryu HJ, Yeo SI, Kang TC. P2 $\times$ 7 receptor differentially modulates astroglial apoptosis and clasmatodendrosis in the rat brain following status epilepticus. *Hippocampus* 2011; **21**: 1318–1333.
26. Schreiber V, Dantzer F, Ame JC, de Murcia G. Poly(ADP-ribose): novel functions for an old molecule. *Nat Rev Mol Cell Biol* 2006; **7**: 517–528.
27. Moroni F, Meli E, Peruginelli F, Chiarugi A, Cozzi A, Picca R *et al.* Poly(ADP-ribose) polymerase inhibitors attenuate necrotic but not apoptotic neuronal death in experimental models of cerebral ischemia. *Cell Death Differ* 2011; **8**: 921–932.
28. Andrabi SA, Kim NS, Yu SW, Wang H, Koh DW, Sasaki M *et al.* Poly(ADP-ribose) (PAR) polymer is a death signal. *Proc Natl Acad Sci U S A* 2006; **103**: 18308–18313.
29. Yu SW, Andrabi SA, Wang H, Kim NS, Poirier GG, Dawson TM *et al.* Apoptosis-inducing factor mediates poly(ADP-ribose) (PAR) polymer-induced cell death. *Proc Natl Acad Sci USA* 2006; **103**: 18314–18319.
30. Pieper AA, Verma A, Zhang J, Snyder SH. Poly (ADP-ribose) polymerase, nitric oxide and cell death. *Trends Pharmacol Sci* 1999; **20**: 171–181.
31. Borges K, Gearing M, McDermott DL, Smith AB, Almonte AG, Wainer BH *et al.* Neuronal and glial pathological changes during epileptogenesis in the mouse pilocarpine model. *Exp Neurol* 2003; **182**: 21–34.
32. Mathern GW, Babb TL, Pretorius JK, Melendez M, Levesque MF. The pathophysiologic relationships between lesion pathology, intracranial ictal EEG onsets, and hippocampal neuron losses in temporal lobe epilepsy. *Epilepsy Res* 1995; **21**: 133–147.
33. Ordy JM, Wengenack TM, Bialobok P, Coleman PD, Rodier P, Baggs RB *et al.* Selective vulnerability and early progression of hippocampal CA1 neuron degeneration and GFAP-positive astrocyte reactivity in the rat four-vessel occlusion model of transient global ischemia. *Exp Neurol* 1993; **119**: 128–139.
34. Maxwell WL, Dhillon K, Harper L, Espin J, MacIntosh TK, Smith DH *et al.* There is differential loss of neurons from the human hippocampus with survival after blunt head injury. *J Neuropathol Exp Neurol* 2003; **62**: 272–279.
35. Schmidt-Kastner R, Ingvar M. Loss of immunoreactivity for glial fibrillary acidic protein (GFAP) in astrocytes as a marker for profound tissue damage in substantia

nigra and basal cortical areas after status epilepticus induced by pilocarpine in rat. *Glia* 1994; **12**: 165–172.
36. Schmidt-Kastner R, Ingvar M. Laminar damage of neurons and astrocytes in neocortex and hippocampus of rat after long-lasting status epilepticus induced by pilocarpine. *Epilepsy Res Suppl* 1996; **12**: 309–316.
37. Represa A, Niquet J, Pollard H, Ben-Ari Y. Cell death, gliosis, and synaptic remodeling in the hippocampus of epileptic rats. *J Neurobiol* 1995; **26**: 413–425.
38. Ridet JL, Malhotra SK, Privat A, Gage FH. Reactive astrocytes: cellular and molecular cues to biological function. *Trends Neurosci* 1997; **20**: 570–577.
39. Chung YH, Joo KM, Lee YJ, Shin DH, Cha CI. Reactive astrocytes express PARP in the central nervous system of SOD(G93A) transgenic mice. *Brain Res* 2004; **1003**: 199–204.
40. Ha HC. Defective transcription factor activation for proinflammatory gene expression in poly(ADP-ribose) polymerase 1-deficient glia. *Proc Natl Acad Sci USA* 2004; **101**: 5087–5092.
41. Ha HC, Hester LD, Snyder SH. Poly(ADP-ribose) polymerase-1 dependence of stress-induced transcription factors and associated gene expression in glia. *Proc Natl Acad Sci USA* 2002; **99**: 3270–3275.
42. Hassa PO, Covic M, Hasan S, Imhof R, Hottiger MO. The enzymatic and DNA binding activity of PARP-1 are not required for NF-kappa B coactivator function. *J Biol Chem* 2001; **276**: 45588–45597.
43. Hassa PO, Buerki C, Lombardi C, Imhof R, Hottiger MO. Transcriptional coactivation of nuclear factor-kappaB-dependent gene expression by p300 is regulated by poly(ADP)-ribose polymerase-1. *J Biol Chem* 2003; **278**: 45145–45153.
44. Hassa PO, Haenni SS, Buerki C, Meier NI, Lane WS, Owen H *et al*. Acetylation of poly(ADP-ribose) polymerase-1 by p300/CREB-binding protein regulates coactivation of NF-kappaB-dependent transcription. *J Biol Chem* 2005; **280**: 40450–40464.
45. Jørgensen MB, Finsen BR, Jensen MB, Castellano B, Diemer NH, Zimmer J. Microglial and astroglial reactions to ischemic and kainic acid-induced lesions of the adult rat hippocampus. *Exp Neurol* 1993; **120**: 70–88.
46. Farez MF, Quintana FJ, Gandhi R, Izquierdo G, Lucas M, Weiner HL. Toll-like receptor 2 and poly(ADP-ribose) polymerase 1 promote central nervous system neuroinflammation in progressive EAE. *Nat Immunol* 2009; **10**: 958–964.
47. Paxinos G, Watson C. *The Rat Brain in Stereotaxic Coordinates*. 3rd edn Academic Press: San Diego, 1997.
48. Brennan AM, Connor JA, Shuttleworth CW. NAD(P)H fluorescence transients after synaptic activity in brain slices: predominant role of mitochondrial function. *J Cereb Blood Flow Metab* 2006; **26**: 1389–1406.
49. Kim JE, Kwak SE, Kang TC. Upregulated TWIK-related acid-sensitive K + channel-2 in neurons and perivascular astrocytes in the hippocampus of experimental temporal lobe epilepsy. *Epilepsia* 2009; **50**: 654–663.

Supplementary Information accompanies this paper on Cell Death and Disease website (http://www.nature.com/cddis)